Supplementary material for: A hemispheric asymmetry in poleward ocean heat transport across climates: implications for overturning and polar warming*

Emily Newsom[a], Andrew F. Thompson[b], Jess Adkins[b], Eric Galbraith[c]

[a] *Department of Physics, University of Oxford, UK*
[b] *Division of Geological and Planetary Sciences, Caltech, USA*
[c] *Earth and Planetary Science, McGill University, Canada*

Residual overturning and buoyancy transport

As described in the Methods and Materials section of the main text, our study defines ocean overturning strength through its residual circulation, defined as

$$\Psi(y,\sigma) \equiv -\int_{-H}^{\zeta}\int_{x_E}^{x_W} \mathbf{v}(x,y,z)\mathcal{H}(\sigma'(\boldsymbol{x})-\sigma)\,\mathrm{d}x\,\mathrm{d}z, \tag{1}$$

where terms are defined in the main text.

In steady state, the residual overturning circulation balances spatial imbalances in both surface buoyancy forcing (generally, water mass formation) and interior mixing (water mass destruction) [1, 2] through interior buoyancy transport. The total northward buoyancy transport supported by $\Psi(y,\sigma)$ is quantified through the buoyancy transport function [1],

$$B(\sigma,y) \equiv \frac{g}{\rho_0}\int_{\sigma'>\sigma} \Psi(\sigma',y)d\sigma'. \tag{2}$$

Here g is gravitational acceleration and ρ_0 is a reference density for the ocean. Through Eq. 2, the residual overturning (across all densities) at a given latitude is constrained by the total buoyancy forcing to its north (or south), and across a circumpolar global integral or within a closed basin. This

*Corresponding author
Email address: emily.newsom@physics.ox.ac.uk (Emily Newsom)

constraint is approximate, and applies to the degree that surface buoyancy fluxes sum to zero, which need not happen due to the non-linear equation of state for seawater. In fact, the ocean gains buoyancy over its global surface through surface fluxes, because the coefficient of thermal expansion is higher [lower] in regions where heat is gained [lost] [3]. This further motivates our focus on the heat budget, which nearly closes (see discussion above and Fig. S2), and is also particularly illustrative of coupling between the Indo-Pacific (a net heat source) and other basins (each net heat sinks, e.g., Fig. 1 and Fig. S2).

Heat transport pathways

To understand pathways of heat transport between basins, we examine the depth-integrated lateral heat transport, **HT**, in Fig. 4, where

$$\mathbf{HT}(x,y) = \int_{-H}^{z} \mathbf{u}(x,y,z)(T(x,y,z) - T_{ref})dz + \int_{-H}^{z} \mathbf{v}(x,y,z)(T(x,y,z) - T_{ref})dz. \tag{3}$$

Here, **u** and **v** are the zonal and meridional residual velocities at each grid point (including the mean and bolus velocity fields). Here, T_{ref} is a reference temperature, [e.g., 4], and is set to the global mean ocean temperature in each state, where $T_{ref} \approx 1.8, 4.3$ and $6.7°$C in the Cold, Warm, and Hot states, respectively. Total (depth-integrated) meridional heat transport into each basin (Fig. 3d) is not altered by choice of reference temperature, so contributions from parameterized sub-mesoscale diffusion (output only only as a full-column depth-integral referenced to $0°$ C) are included in Fig. 4d.

Changes in the depth structure of meridional heat transport is also strong evidence of evolving inter-basin overturning pathways (Fig. S6). The zonally-summed meridional heat transport, below a given depth z, and across latitude y — the MHT — sheds light on the interior heat transport pathways, and is calculated as

$$\mathrm{MHT}(y,z) = \int_{-H}^{z} \int_{x_E}^{x_W} \mathbf{v}(x,y,z)(T(x,y,z) - T_{ref})dxdz, \tag{4}$$

Here, x_E and x_W are the eastern and western boundaries of the domain (basin or full longitude circle), and v and T are the local velocity and temperature, respectively. Here a parameterized bolus contribution is added to

the velocity field, and thus MHT should include eddy-induced heat transport. Here, T_{ref} is a reference temperature, e.g., [4]. Note that MHT does not include contributions to the heat transport from other parameterised sub-mesoscale processes, since only the depth-integral of these contributions were saved in the model output. In Fig. S6, we evaluated the MHT at 30°S by setting T_{ref} to T_{ref} to the global mean ocean temperature in each state, as above. The anomaly in MHT$(-30, z)$ between states, Fig. S6b,d, illustrates how the depth structure of heat transport — its depth penetration — is altered with climate warming. The MHT can be calculated at any latitude; contours in its spatial distribution can be interpreted as pathways of heat transport through the interior. Coherence in MHT and B (Eq. 3) indicate how strongly advective heat transport contributes to the total interior buoyancy transport. These fields are compared in Fig. S6. The choice of reference temperature should not alter the total meridional heat transport at the surface, across a given latitude, *i.e.* MHT$(y, 0)$. In Fig. S4d, MHT$(-30, 0)$ does include contributions from parameterized sub-mesoscale diffusion, which, again, were saved only in their depth-integral and referenced to 0° C.

References

[1] E. R. Newsom, A. F. Thompson, Reassessing the Role of the Indo-Pacific in the Ocean's Global Overturning Circulation, Geophysical Research Letters 45 (2018) 422–12. doi:10.1029/2018GL080350.

[2] S. Groeskamp, S. M. Griffies, D. Iudicone, R. Marsh, A. G. Nurser, J. D. Zika, The Water Mass Transformation Framework for Ocean Physics and Biogeochemistry, Annual Review of Marine Science 11 (2019) 271–305. doi:10.1146/annurev-marine-010318-095421.

[3] J. J. Schanze, R. W. Schmitt, Estimates of Cabbeling in the Global Ocean, Journal of Physical Oceanography 43 (2013) 698–705. URL: `http://journals.ametsoc.org/doi/abs/10.1175/JPO-D-12-0119.1`. doi:10.1175/JPO-D-12-0119.1.

[4] X. Xu, P. B. Rhines, E. P. Chassignet, Temperature–Salinity Structure of the North Atlantic Circulation and Associated Heat and Freshwater Transports, Journal of Climate 29 (2016) 7723–7742. URL:

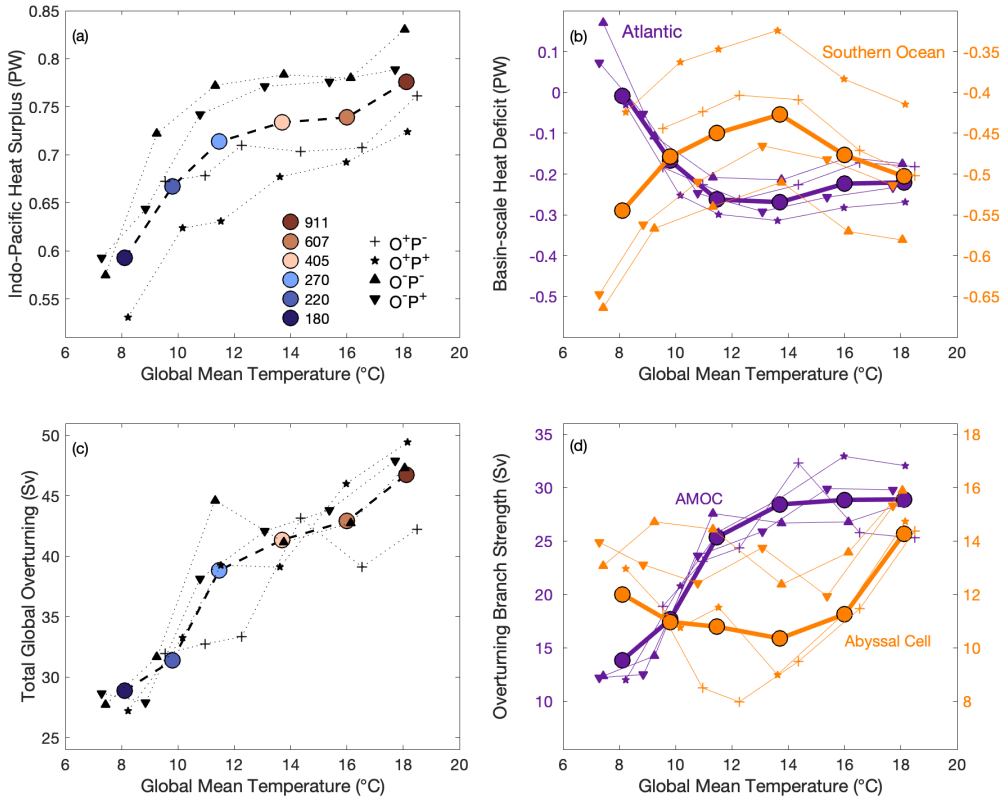

Figure 1: The colored points reproduce the information in Fig. 1; the individual dotted lines show the trajectory of the various diagnostics for each of the four different orbital forcing combinations (see Model Description above) as a function of GMT and increasing CO_2. Each curve is labeled to indicate the precession angle ($P^+ = 270°$, $P^- = 90°$) and obliquity angle ($O^+ = 24.5°$, $O^- = 22°$). Although there is an offset between different orbital forcing simulation suites, trends with increasing GMT are qualitatively similar.

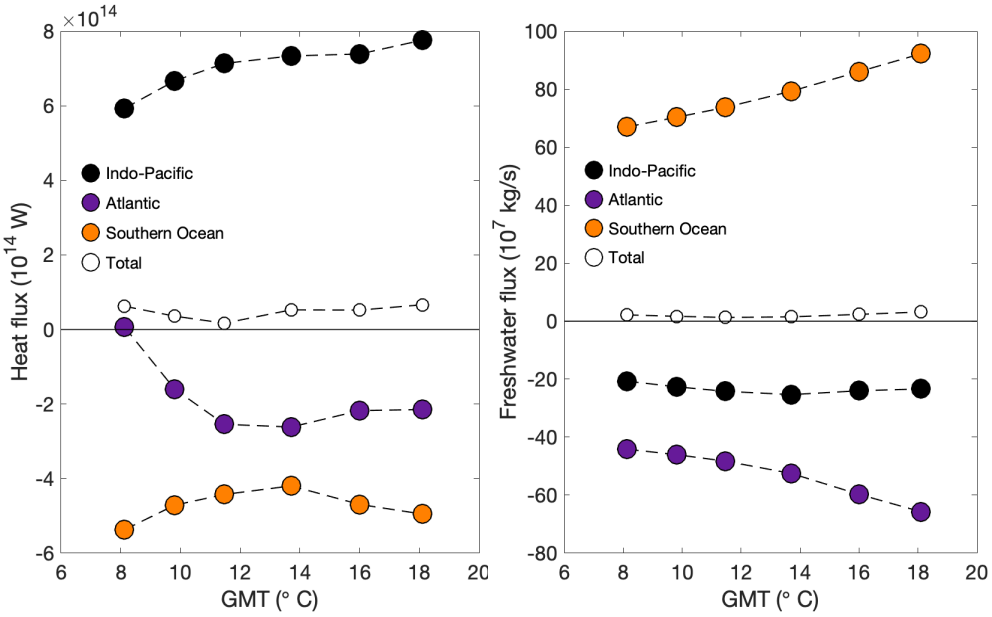

Figure 2: Surface heat, freshwater, and buoyancy flux. Total surface heat fluxes (a) and total surface freshwater flux (b) integrated over the Indo-Pacific (black), Atlantic (purple) and Southern Ocean (orange). The total surface flux over the globe is given in white in each panel. Note a slight global imbalance in heat flux across all states (order $\sim 10^{13}$ W). The global freshwater budget is very close to closure.

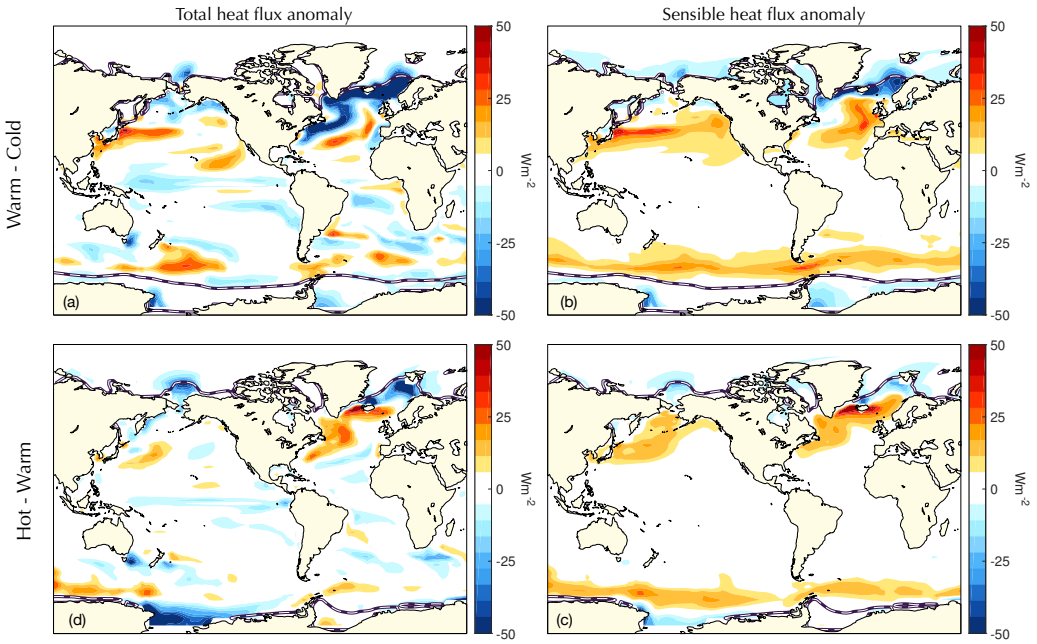

Figure 3: Summary of the shifting distribution of surface heat flux. Spatial distribution of total surface heat flux anomaly between the Warm and Cold states (a) and Hot and Warm states (b). Same, but showing the spatial distribution of the anomalous sensible heat flux alone (c-d). Here positive is into the ocean. The black contour overlaid on each represents the extent of the sea ice pack (of concentration of 10% or greater) in the Warm (a)-(b) and the Hot (c)-(d) states.

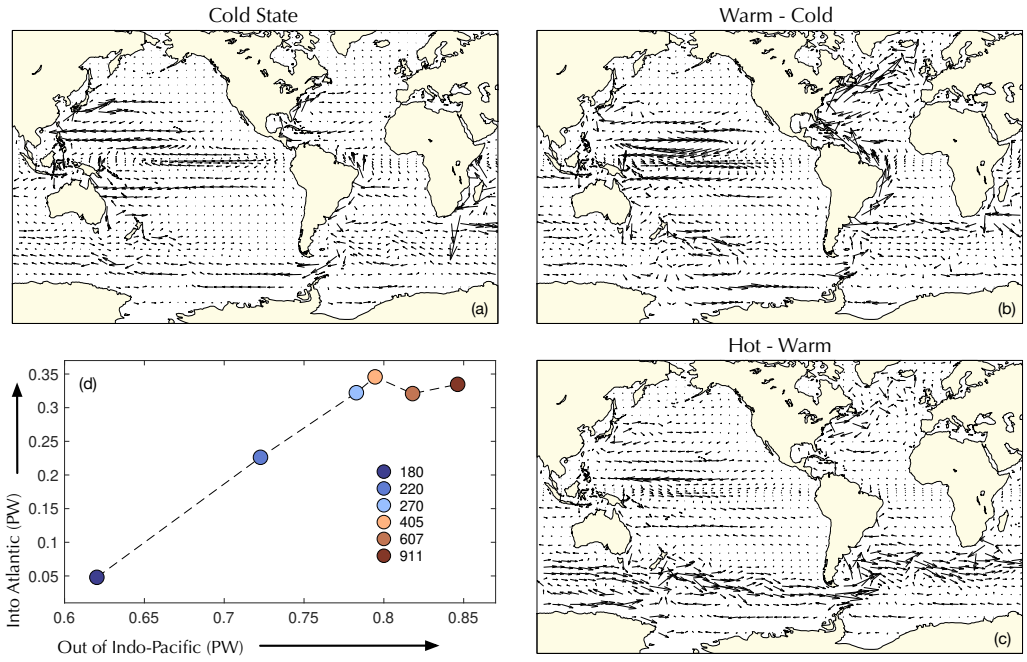

Figure 4: Summary of inter-basin heat transport pathways. (a) Vectors indicating the relative magnitude and direction of depth-integrated heat transport, **HT** (PW), in the cold state (Eq. 3; see Methods) Panels (b) and (c) show the anomaly in heat transport (Δ**HT**) between the Warm and Cold states and the Hot and Warm states, respectively. Heat transport is referenced to global mean ocean temperature: $T_{ref} \approx 1.8, 4.3$ and $6.7°$C in the Cold, Warm, and Hot states. (d) The total meridional heat transported across 30°S out of the Indo-Pacific versus into the Atlantic. The color of the circle indicates the atmospheric CO_2 level (ppm). This panel shows that, while heat transport out of the Indo-Pacific increases across all states, transport into the Atlantic only increases between the Cold and Warm states.

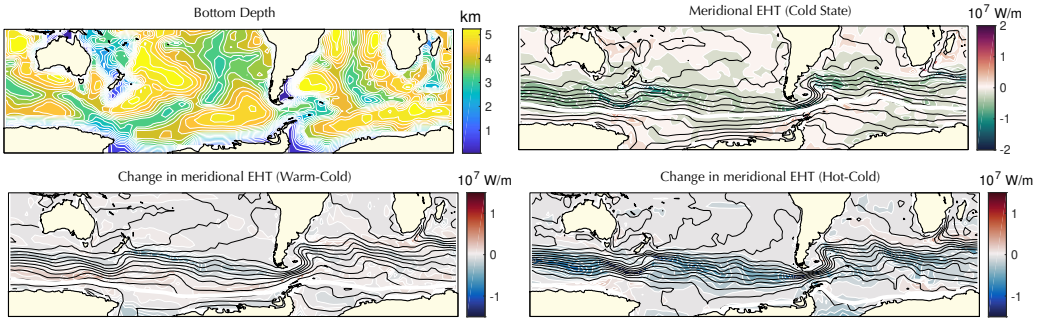

Figure 5: Changing meridional eddy heat transport (EHT) patterns. Top left: bottom depth of the Southern Ocean (km). Top right: Cold state pattern of eddy heat transport (colored contours) and contours of SSH (black lines) in the Southern Ocean. Here, $EHT = \int_z v_{GM}(T - T_{ref})dz$. Bottom left: change in EHT, Warm - Cold. Bottom Right: change in EHT, Hot - Cold.

http://journals.ametsoc.org/doi/10.1175/JCLI-D-15-0798.1.
doi:10.1175/JCLI-D-15-0798.1.

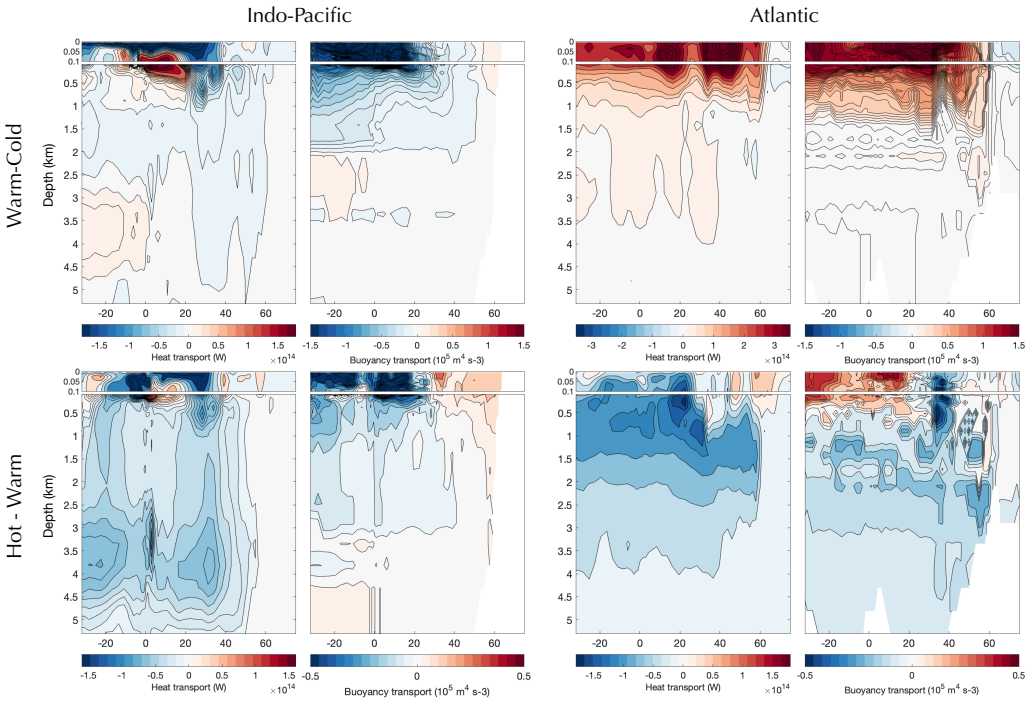

Figure 6: Anomalous interior heat and buoyancy transport patterns. The upper panels show differences between the Warm and Cold states (warm - cold); the lower panels show differences between the Hot and Warm states (Hot - Warm). Left: anomalies in MHT (Eq. 4) and B (Eq. 2) in the Indo-Pacific; Right, same but in the Atlantic. Note for B, density anomaly σ is referenced to 2000 m. Streamlines of MHT and B should be interpreted as changes in interior pathways of meridional heat and buoyancy transport, respectively. Both show a deepening of heat and buoyancy export from the Indo-Pacific with warming.

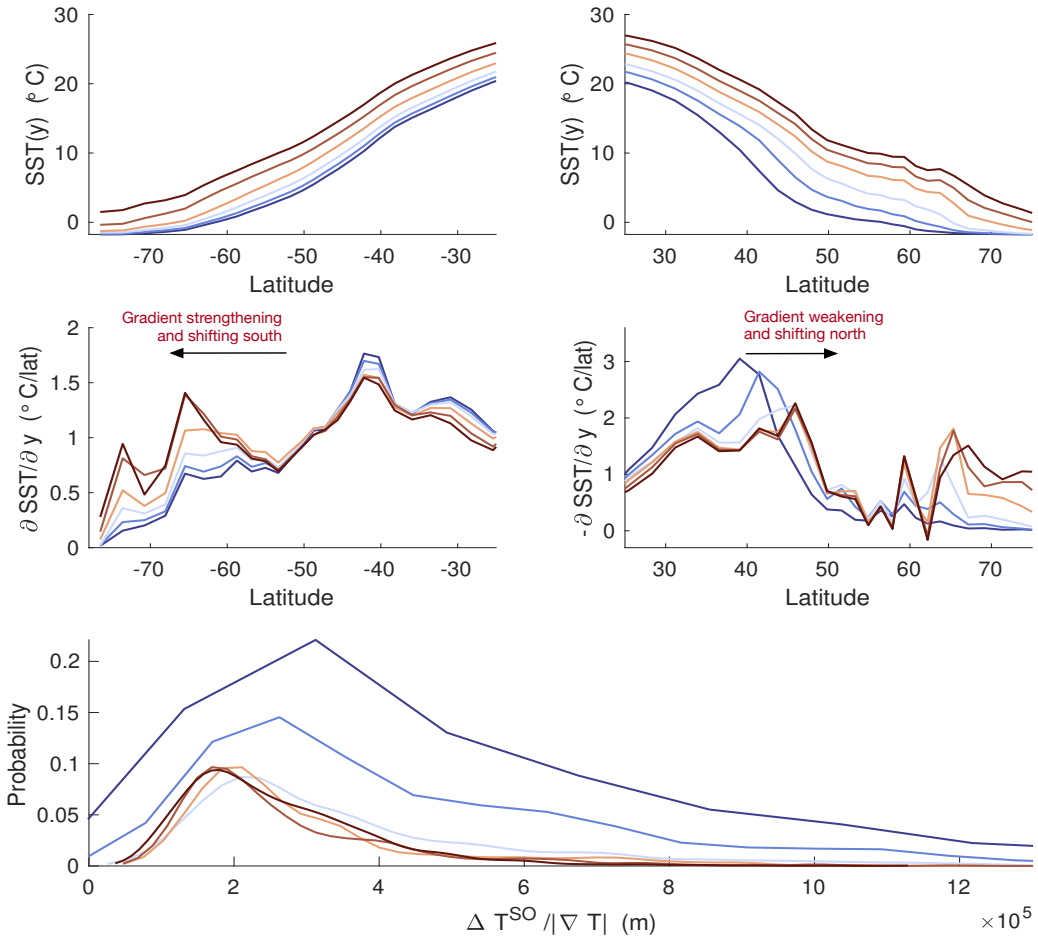

Figure 7: Summary of parameters used in scaling relationships (Eqs. 1-6 in the main text) Top row: zonal mean SST and zonal mean meridional SST gradient with climate state, south of 25° S (left) and north of 25° N (right). Middle row: meridional SST gradient in corresponding regions. Note, around 40° S, a second peak in the gradient represents the ACC's northern boundary. Also note, in this hemisphere, temperatures generally increase with latitude. Bottom row: distribution of length-scales associated with characteristic ΔT^{SO}, or $\Delta T^{SO}/|\nabla T|$, for region south of 50°S; note that tails of distributions aren't show, and are longer in warmer states, explaining different magnitude in peaks.

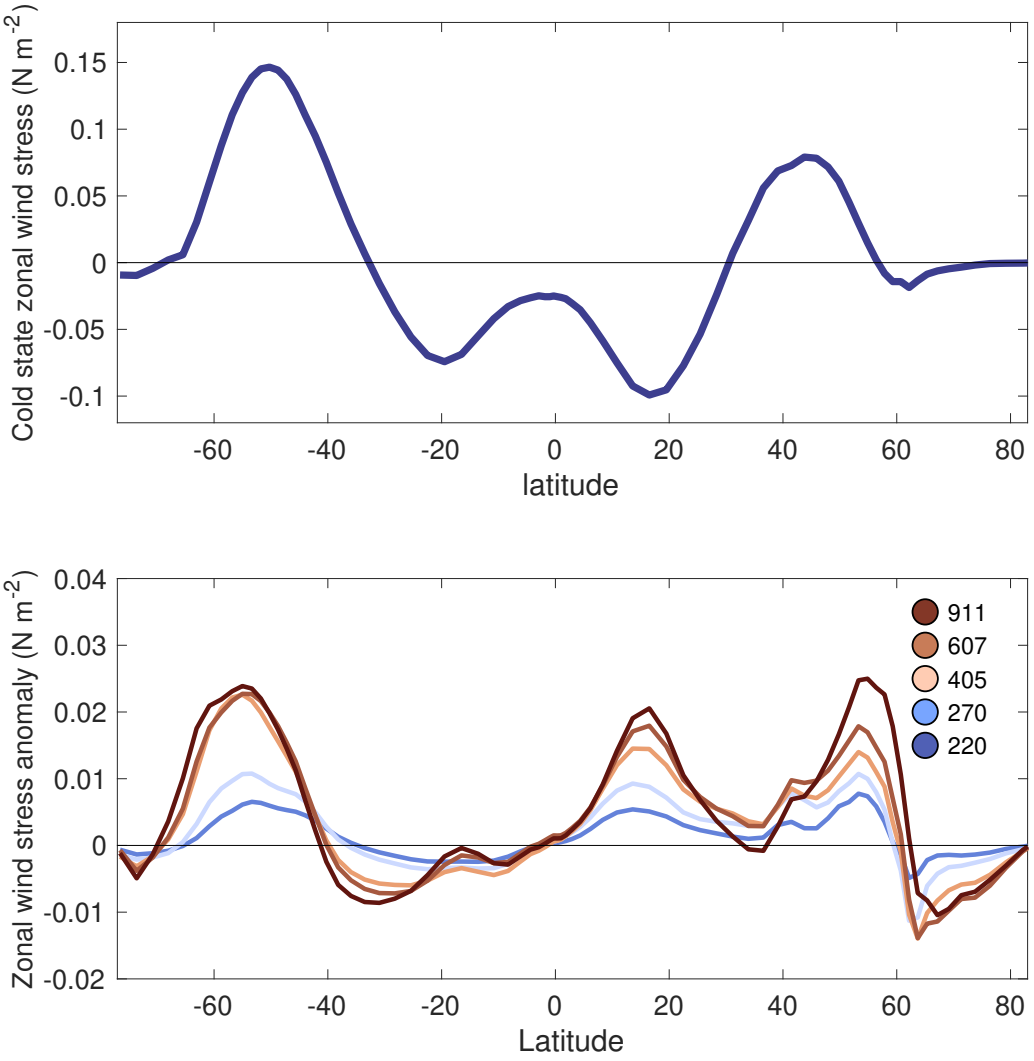

Figure 8: Summary of changes in wind stress patterns across climate states. Top) zonally-averaged zonal wind stress (Nm^{-2}) in the cold state. Bottom) anomaly in zonally-averaged zonal wind stress (Nm^{-2}) from cold state values in warmer states. Colors indicate the atmospheric CO_2 level (ppm). These anomalies show a general poleward expansion of westerly wind stress bands, and an associated poleward shift in westerly wind stress maxima, in both hemispheres with climate warming.